Comparison of Fault Detection Techniques for an Ocean Turbine

Mustapha Mjit, Pierre-Philippe J. Beaujean, and David J. Vendittis

Florida Atlantic University, SeaTech, 101 North Beach Road, Dania Beach, FL 33004 USA
mmjit@fau.edu
pbeaujea@fau.edu
dvendittis@aol.com

ABSTRACT

The Southeast National Marine Renewable Energy Center at Florida Atlantic University, which supersedes the Center for Ocean Energy Technology (Driscoll et al., 2008), is conducting research and development to support the implementation of ocean current and ocean thermal energy technologies for a low environmental-impact extraction of energy.

Fault detection capability is needed for these offshore ocean turbines (and other systems) because access to these machines for maintenance is difficult and costly. Techniques that offer reliable and early (incipient) detection allow for preventive maintenance to prevent the development of secondary faults that may be generated by the primary faults. Several methods for processing and displaying vibration data are compared and evaluated relative to synergistic detection utilizing data from a prototype (dynamometer) of an ocean current turbine. The results may generically apply to other machines, such as wind turbines.[1]

1. INTRODUCTION

An ocean turbine (OT) is subject to high and varying loads, locations that are difficult to access and extreme environment conditions; therefore, it requires special predictive monitoring strategies (Sloan et al., 2009; Beaujean et al., 2009). For many machines, a vibration condition monitoring program is considered as one of the most important tools to detect the presence of anomalous behavior, thus allowing for early remedial actions to reduce both maintenance costs and premature breakdown. Since access is difficult and costly, monitoring techniques that detect these faults reliably (and early) for machines like offshore ocean turbines offer an advantage over the more standard techniques (e.g. vibration level trending), allowing for preventive maintenance and to prevent the development of secondary faults that may be initiated by the primary faults.

This paper discusses several approaches, procedures and techniques considered to detect and diagnose the faults of an ocean turbine, utilizing vibration data. Specifically, modulation detection techniques utilizing the Cepstrum or the Hilbert transform and transient detection techniques (Short Time Fourier Transform (STFT) and kurtosis) are considered. Such methods have shown to be efficient, (Fernandez et al., 2005; Kim et al., 2006), for detecting faults that affect the component health of machines (e.g. motors, gearboxes, fans and generators) generically similar to those that may be considered subsystems of an OT (Figure 1).

A LabVIEW model for on-line vibration condition monitoring was developed (Mjit, 2009; Mjit et al., 2010). It contains the advanced fault detection techniques mentioned above as well as diagnostic techniques that provide information about the type, severity and identification of the fault. The principal monitoring method utilizes the Power Spectral Density (PSD) for in-depth analysis of the vibration signal and for vibration level trending, assuming acceptable stationary of the vibration signal. The model was exercised using data acquired from a rotor end of a dynamometer (Figure 2), which is representative of the electrical and mechanical equipment of the actual OT (Figure 1). The data were processed in several different ways to evaluate the relative ability of the detection techniques to detect the types of incipient faults expected of the OT. Actual turbine data may differ because of the presence of the dynamometer's motor drive and additional gearbox. Varying loads and structural fluid loading of the OT may affect the frequency of structural resonances; however the types of mechanical faults should be generically the same. The purpose of this effort was to determine if the conclusions and recommendations made in (Fernandez et al., 2005; Kim et al., 2006) apply to the dynamometer and, possibly, the OT.

Most machines display some non-stationary behavior, mainly because of varying loads or structural variations. This affects the vibration data (Fernandez et al., 2005), mainly by causing frequency shifts. Because of the additional variations caused by changes in the water current velocity, it is expected that the vibration data collected from the ocean turbine will be even less stationary in nature than those from the dynamometer. Therefore, the use of wavelets, possibly combined with other algorithms, such as the Hilbert transform, may be necessary to assess changes in the vibration levels, (Fernandez et al., 2005; Fan et al., 2006; Tyagi et al., 2003; Wald et al., 2010). Such a combination is under development and will be evaluated with the in-water turbine data.

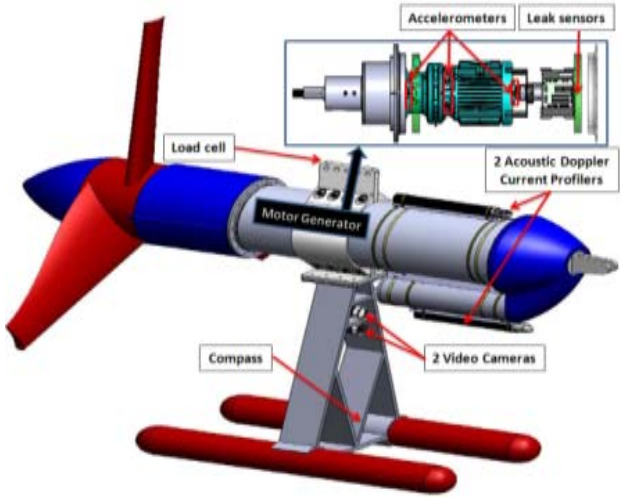

Figure 1. Ocean Turbine, Conceptual.

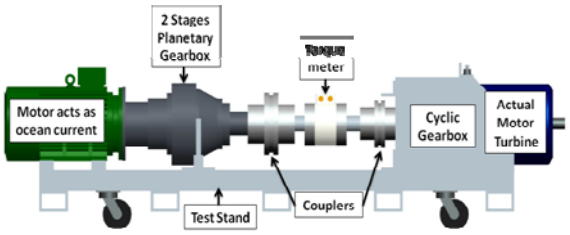

Figure 2. Dynamometer.

2. LISTING AND DESCRIPTION OF THE FAULT DETECTION TECHNIQUES

2.1 Power Spectral Density and Fractional Octave Analysis

The PSD is derived from the vibration time waveform by performing a Fast Fourier Transform (FFT). The PSD is well-suited to analysis and diagnosis as it shows more clearly the forcing frequencies of the rotating components. This technique is very accurate for stationary machines. The PSD is averaged over fractional octave bands, and is used for trending and detection as it covers a large frequency range. The trending of fractional octave spectra is very accurate especially if there is small speed variation. The PSD is also very accurate for stationary machine where the forcing frequencies of the components do not vary with time. The PSD can also be used for (slightly) non-stationary machines if one is only interested in the spectral components that exist in the signal, but not interested in what time each spectral component occurs. Most of the peaks in the PSD are directly proportional to the running speed of the machine. The PSD may be normalized during each iteration before the averaging process to avoid smearing in the case of non stationary machine speeds.

2.2 Cepstrum Analysis

The power cepstrum is the inverse FFT of the logarithm of the power spectrum of a signal; it is used to highlight periodicities in the vibrations spectrum, in the same way that the spectrum is used to highlight periodicities in the time waveform. Thus, harmonics and sidebands in the spectrum are summed into one peak in the cepstrum (called rahmonic), allowing identification and trending of modulation frequencies associated with a specific fault.

$$C(f) = \int_{-\infty}^{+\infty} \log\left(\left|F\{x(t)\}\right|^2\right) \times e^{-j2\pi s/f}\, ds. \qquad (1)$$

F is the Fourier transform operator; $x(t)$ is the time signal and f is the frequency in hertz.

2.3 Kurtosis

Kurtosis is a statistical parameter, derived from the fourth statistical moment about the mean of the probability distribution function of the vibration signal and is an indicator of the non-normality of that function. The kurtosis technique has the major advantage that the calculated value is independent of load or speed variations. The kurtosis analysis is good for faults and transient effect detection, but it does not give an indication of the specific source of the problem (Reimche et al., 2003); however, the kurtosis will diminish with increased distance from the source of the transients. The kurtosis will be equal to 3 for a healthy machine and greater than 3 if the machine‘s vibrations contain transients. The general definition of the kurtosis is,

$$Kurtosis = \frac{\sum_{i=1}^{n}\left(x_i - \bar{x}\right)^4}{\left(n-1\right)\sigma^2} \qquad (2)$$

The variables $x_1, x_2 .. \ x_n$ represent the population data of the signal, $\overline{x}$ is the mean of x, σ is the variance of x and n is the number of samples.

2.4 Hilbert Transform Analysis

The Hilbert transform of a real signal is defined as the convolution of the signal with the function 1/πt,

$$\hat{x}(t) = \frac{1}{\pi} \int_{+\infty}^{-\infty} \frac{x(\tau)}{t-\tau} d\tau. \quad (3)$$

The complex analytic signal is:

$$\tilde{x}(t) = x(t) + j\hat{x}(t). \quad (4)$$

The envelope of the original signal is defined as follow:

$$e(t) = \tilde{x}(t)\ e^{-j2\pi ft}. \quad (5)$$

f is the frequency of the modulated signal.

The Hilbert transform is used to demodulate the signal so as to obtain the low frequency variations (faulty signal) in a higher frequency signal (forcing or resonance frequency). When a fault starts developing, the vibrations caused by a bearing or gear fault is obscured (especially at low frequency) by the noise or the vibrations from other rotating parts like shafts, gears, etc. In this case, the bearing or gear frequencies cannot be seen in either the time waveform or the spectrum of the vibration. The Hilbert transform can be used to highlight and extract the modulating signal (faulty signal) from the modulated signal (characteristic frequency of the machine). The Hilbert transform technique removes the carrier signals which are of no interest for fault detection. Amplitude modulation occurs for example when a gear rides on a bent or misaligned shaft, while frequency modulation occurs for example when the shaft speed varies with time. In the case of a narrow-band detection process, a band-pass filter (whose pass band includes the fault frequencies) filters out the selected part of the spectrum. The output is shifted (heterodyned) to low frequency and subjected to envelope detection.

$$BSP(f, f') = \int_{-\infty}^{+\infty} \int_{-\infty}^{+\infty} \tilde{x}(\tau) w_1(t,\tau) e^{-j2\pi(f'\tau + ft)} d\tau dt \quad (6)$$

BSP is the bispectrum of the analytical signal $\tilde{x}$, f and f' are the modulated and modulating frequencies respectively. w_1 is a time window.

2.5 Short Time Fourier Transform

For non-stationary machines, the Short Time Fourier Transform (STFT) of the signal should be used to clearly identify non-stationary vibration data related to speed variation, from vibrations caused by the inception of anomalies, Indeed, the PSD may not provide sufficient information about the presence of transient effect, since abrupt change in the time signal is spread out over the entire frequency range. Time-frequency Analysis results are displayed in a spectrogram, which shows how the power of a signal is distributed in the time-frequency domain. Narrow-band, periodic signals, transients and noise appear very distinctly on a spectrogram. The STFT is based on the following mathematical operations,

$$PS(t, f) = \left| \int_{-\infty}^{+\infty} x(t') w_2(t' - t) e^{-j2\pi ft'} dt' \right|^2 \quad (7)$$

PS is the power spectrogram of the signal $s(t)$ and $w_2(t)$ is a real and symmetric window translated by *t*. t and f are the instantaneous time and frequency.

3. DATA ACQUISITION

Vibration data were acquired from the dynamometer running at various RPM with simulated faults to evaluate the ability of the detection algorithms to detect the presence of incipient faults. Processing features such as stationary assumptions and smoothing windows were also evaluated to insure a high quality for the data. The faults were simulated for selected levels of severity to determine whether the conclusions depended on existing signal-to-noise levels. Note that the motor and second gearbox (simulated rotor) section of the dynamometer were detached and instrumented (Figure 3). The motor was operated at selected speeds with and without several weights that increased the rotor shaft imbalance. These tests were performed to evaluate the envelope analysis using Hilbert, the PSD and cepstrum techniques. Additionally, a hammer was used to introduce impact transients. The response of the monitoring system to such impacts was evaluated using the kurtosis and the STFT. The anomaly detection techniques were implemented and assessed relative to their detection capabilities.

In this paper, the motor was operated at 1,144 RPM under normal and augmented imbalance condition. The shaft rotated at 52.47 RPM due to the reduction ratio (1:21.8) of the two stages reduction planetary gearbox. The expected mechanical forcing frequencies (Singleton, 2006) relative to the motor speed of 1,144 RPM are summarized in Tables 1 and 2. These forcing frequencies are calculated

automatically in the LabVIEW program. Note that Tables 1 and 2 show only the fundamental forcing frequencies and not their harmonics.

The experiment was performed on the rotor section of the dynamometer in three different situations: without any weight added to the shaft, with a light weight (two magnets, 0.5 lbs total) and with a large weight (two magnets and two blocks, 2.875 lbs total) attached to the very end of the output shaft. The distance from the shaft axis to the location of the weights was 3.7 inches. Changes in third octave bands, power spectral density, envelope and kurtosis were measured. The acceleration data were collected using a Low Frequency (0.2 to 3000 Hz) piezoelectric accelerometer with a sensitivity of 500 mv/g mounted on the torque meter. The sampling frequency F_s was 5,000 Hz or 20,000 Hz. The number of data points in each sample was 20,000. The corresponding frequency resolution was 0.25 Hz (at F_s = 5,000 Hz) or 1 Hz (at F_s = 20,000 Hz). A total of 500,000 points were acquired (25 samples). A Hanning window was used to smooth the data.

4. PSD, HILBERT AND CEPSTRUM ANALYSES

Figures 4 to 6 show the baseline (without imbalance condition introduced) PSD, in three different frequency regions, of the data acquired at 1,144 RPM of the motor. The major frequency components (derived from the known forcing frequencies) are identified in these figures. These forcing frequencies are tabulated in Table 3. In figure 4, the average of the PSD (25 samples) in the low frequency region (0.5 to 50 Hz) was calculated using 500,000 data points (20,000 for each sample) for a sampling rate of 5,000 Hz to achieve a frequency resolution of 0.25 Hz. High frequency resolution was needed in the low frequency region (below 50 Hz) as the forcing frequencies are closer to each other. In Figures 5 and 6, the average of the PSD (25 samples) in medium and high frequency region - calculated using 500,000 data point for a sampling rate of 20,000 Hz (20,000 points per sample) and a frequency resolution of 1 Hz - are shown. Figure 7 shows the baseline PSD of the motor running at two different speeds (not harmonically related), 1,144 RPM and 1,593 RPM; this allows for the identification of the resonant frequencies of the system as both PSD should display the same peaks at these frequencies.

	1st stage planetary gear	**2nd stage planetary gear**
Carrier speed	3.57 RPS	0.87 RPS
Planet speed	9.62 RPS	2.70 RPS
Planet absolute speed	6.04 RPS	1.82 RPS
Planet gear mesh frequency	279.02 Hz	59.47 Hz
Sun gear mesh frequency	343.2 Hz	78.69 Hz
Planet passing frequency	10.73 Hz	2.62 Hz
Sun gear side band defect frequency	46.46 Hz	8.10 Hz
Planet gear side band defect frequency	19.24 Hz	5.40 Hz

Table 1. Expected forcing frequencies from planetary gears of the rotor side of the dynamometer, motor speed 1,144 RPM (19.06 Hz).

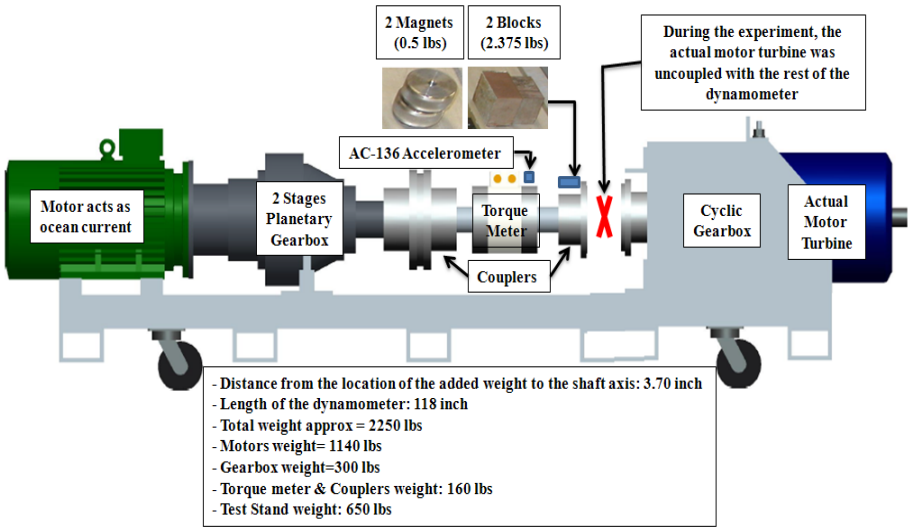

Figure 3. Rotor end of the Dynamometer.

	Bearing 1	Bearing 2	Bearing 3
Outer ring frequency	58.58	58.26	7.69
Inner ring frequency	93.95	94.26	13.29
Roller bearing frequency	77.80	76.29	3.03
Cage frequency	7.32	7.28	0.32

Table 2. Expected forcing frequencies (in Hz) from bearings of the rotor side of the dynamometer, motor speed 1,144 RPM (19.06 Hz).

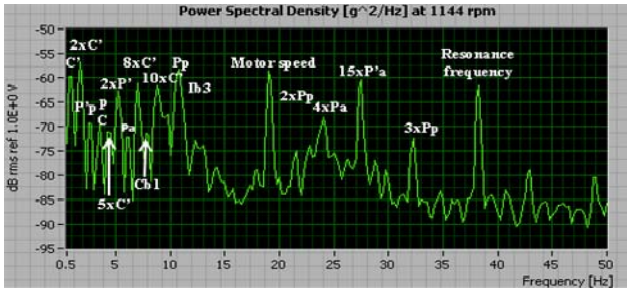

Figure 4. Forcing frequencies identification on the PSD plot (0.5 Hz to 50 Hz).

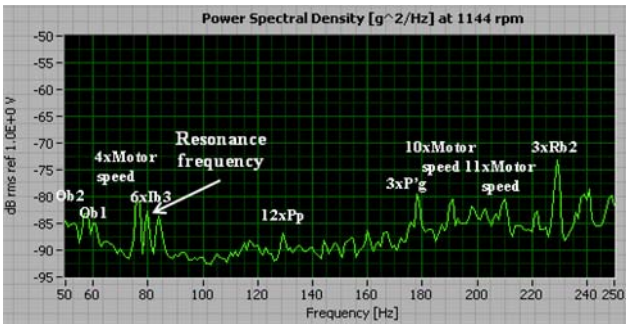

Figure 5. Forcing frequencies identification on the PSD plot (50 Hz to 250 Hz).

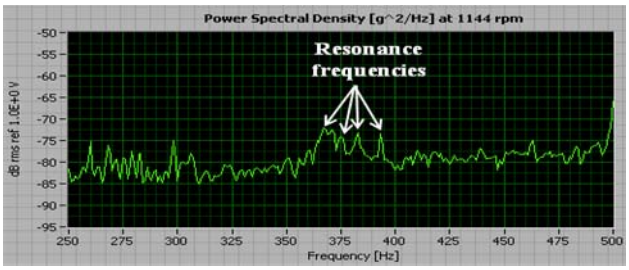

Figure 6. Forcing frequencies identification on the PSD plot (250 Hz to 500 Hz).

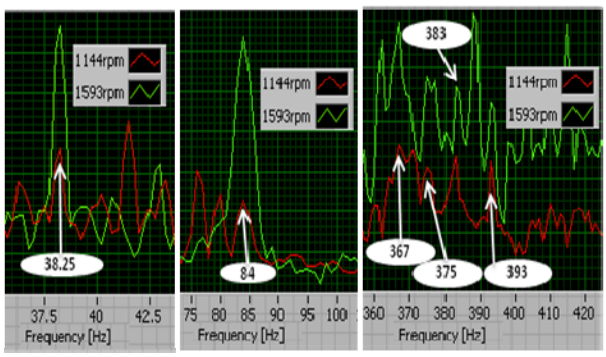

Figure 7. The PSD at 1,144 RPM and 1,593 RPM show the same peaks at resonance frequencies.

In Figure 8, the difference in levels between the imbalance and baseline in the third octave bands (63 Hz, 125 Hz, 160 Hz, 200 Hz, 250 Hz and 315 Hz) exceed the threshold (level increase allowance) of 5dB, causing the alarm for each of those third octave bands to switch on. In figure 9, the PSD and the spectrograms clearly show peaks at about 60 Hz and 120 Hz relative to the modulation in the case of extreme imbalance. The increase in level is due to the imbalance of the shaft that causes the planet gear meshing frequency (59.5 Hz) and its harmonics (119 Hz, 178.5 Hz) to be modulated by the rotational frequency (0.88 Hz) and its harmonics (1.76 Hz, 2.64 Hz, 3.52 Hz) (Figure 11); for brevity, only the modulation of the fundamental planet gear meshing frequency is shown. Similar conclusions were made from data acquired with the motor running at 1,593 RPM. Figure 10 shows comparisons between imbalance effect on the PSD and Hilbert envelope analyses.

The Hilbert envelope analysis shows the major modulation of the gear meshing frequency much more clearly than the PSD do. Table 4 summarizes the amplitude change relative to the baseline using the third octave, PSD and Hilbert envelope analysis, in the case where the unbalance is caused either by two magnets attached to the shaft or two magnets and two blocks attached to the shaft. The table shows that the PSD levels and the levels of the demodulating frequencies (envelope analysis) increased with imbalance condition. Figures 11 and 12 show the PSD and the spectrograms with two magnets attached to the shaft, and two magnets and two blocks, in the frequency ranges 130-250 Hz and 215-500 Hz, respectively. The spectrograms show clearly the peaks (at the modulating frequencies and it harmonics) that are causing the third octave bands shown in figure 8 to exceed their baselines. The kurtosis was not affected by the imbalance at either speed, but would have changed significantly if the imbalance was causing damage to the gears or bearings – an example of data fusion and a potential tool for prognosis.

Freq.	Forcing frequencies	Symbol
19.06	Motor speed	-
0.87	Shaft speed 2nd stage gear	C’
3.57	Shaft speed 1st stage gear	C
2.62	Planet passing frequency 2nd stage	P’p
10.73	Planet passing frequency 1st stage	Pp
1.82	Planet absolute frequency 2nd stage	P’a
6.04	Planet absolute frequency 1st stage	Pa
178	Planet gear mesh frequency 2nd stage	P’g
7.32	Cage defect frequency 1st bearing	Cb1
58.58	Outer race defect frequency bearing 1	Ob1
58.26	Outer race defect frequency bearings 2	Ob2
7.69	Inter race defect frequency bearings 3	Ib3
76.29	Roller bearing frequency bearing 2	Rb2
38.25, 84, 367, 375, 383, 393	Resonance frequencies	-

Table 3. Observed forcing frequencies (in Hz) in the PSD for motor running at 1,144 RPM (19.06 Hz).

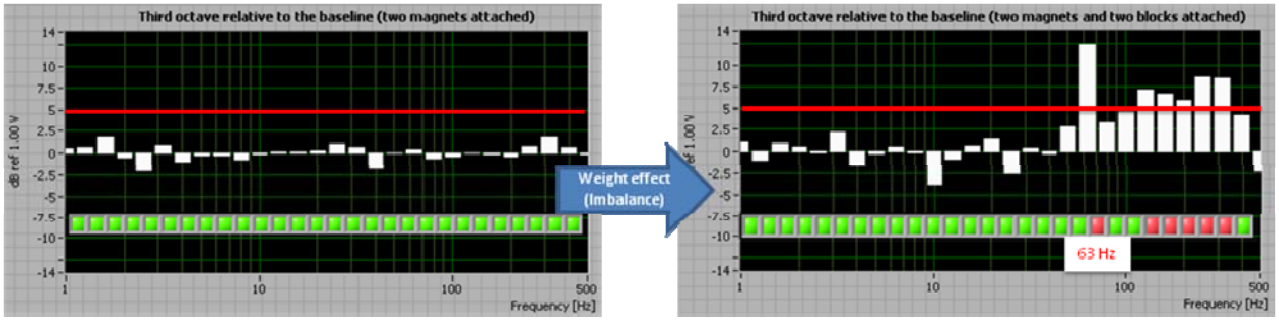

Figure 8. Relative amplitude with respect to the baseline (normal condition) using third-octave analysis; two magnets attached to the shaft (left) and, two magnets and two blocks (right).

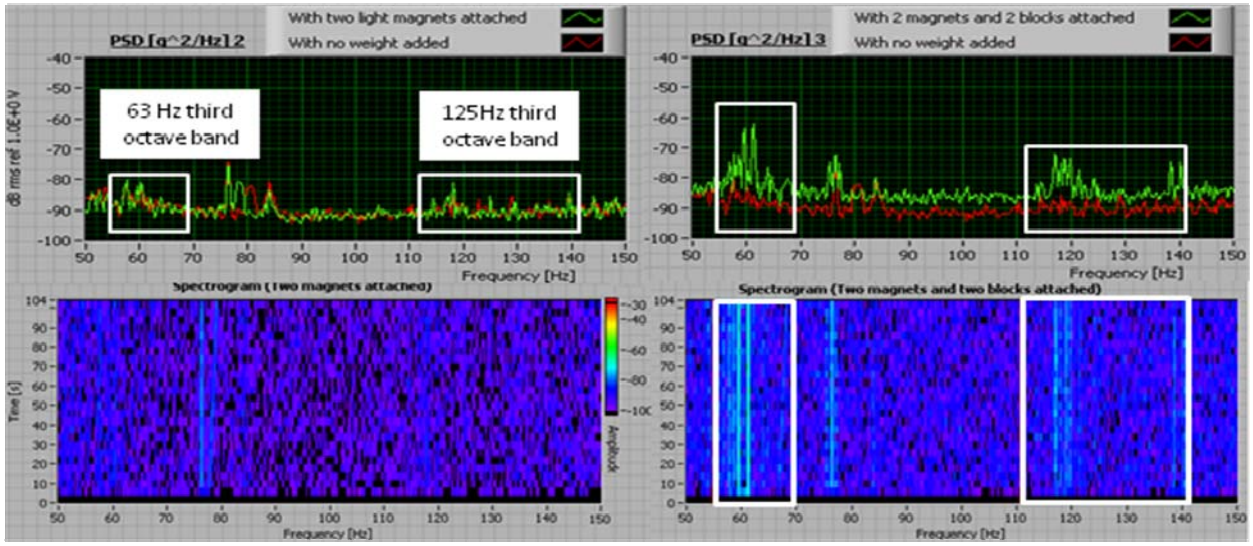

Figure 9. Power spectral density and spectrogram in the frequency range 50-150 Hz, with two magnets attached to the shaft (left) and two magnets and two blocks (right).

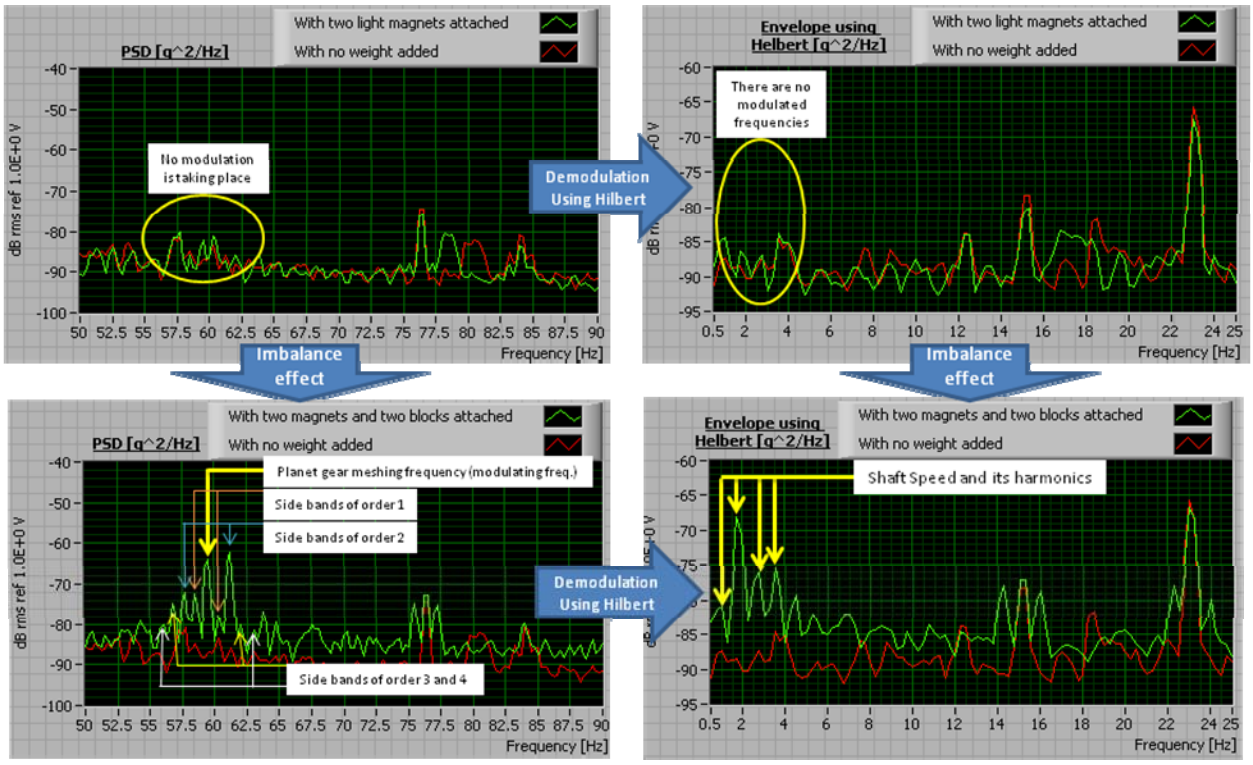

Figure 10. Power spectral density and its Hilbert envelope analysis; two magnets attached to the shaft (top) and two magnets and two blocks (bottom).

	Two magnets					Two magnets & Two blocks				
	59.5Hz tone	1st order sideband	2nd order sideband	3rd order sideband	4th order sideband	59.5Hz tone	1st order sideband	2nd order sideband	3rd order sideband	4th order sideband
PSD relative level (dB)	4.63	2.37	-1.34	2.35	3.31	23.04	5.82	23.59	8.26	5.21
Hilbert envelope relative level (dB)		2.87	0.19	-0.4	0.04		11.11	18.17	6.5	6.37
1/3octave Analysis (dB)	0.92 (relative level in the 63Hz third octave band)					12.47 (relative level in the 63Hz third octave band)				

Table 4. Comparison of the features (PSD, envelope and third octave level) relative to the baseline (no weight added), for two levels of unbalance severity, one with two light magnets, and another with two magnets and two blocks.

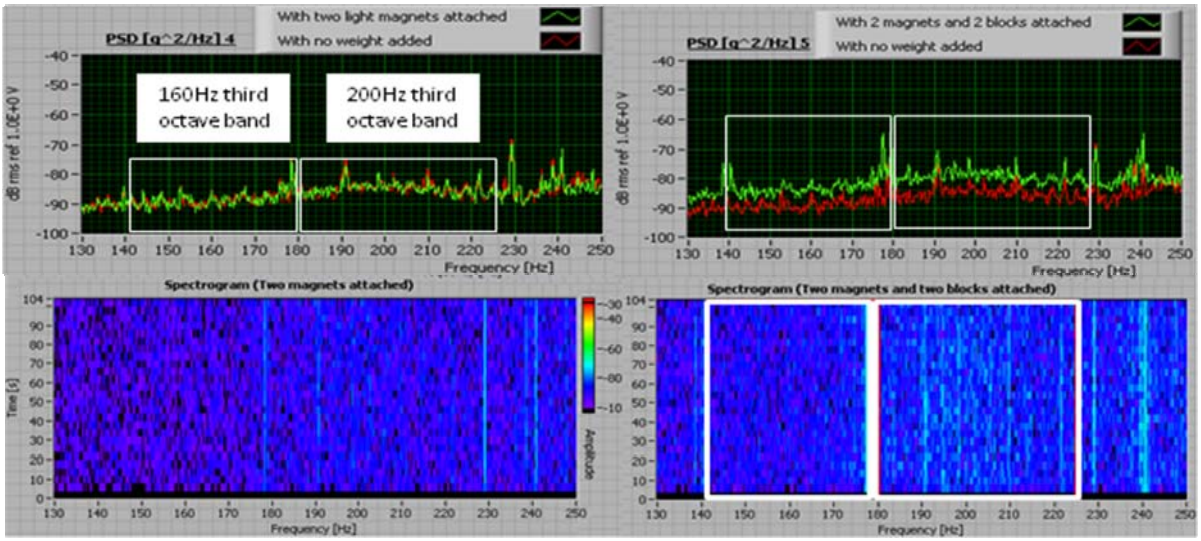

Figure 11. Power spectral density and the spectrogram in the frequency range 130-250 Hz, with two magnets attached to the shaft (left) and two magnets and two blocks (right).

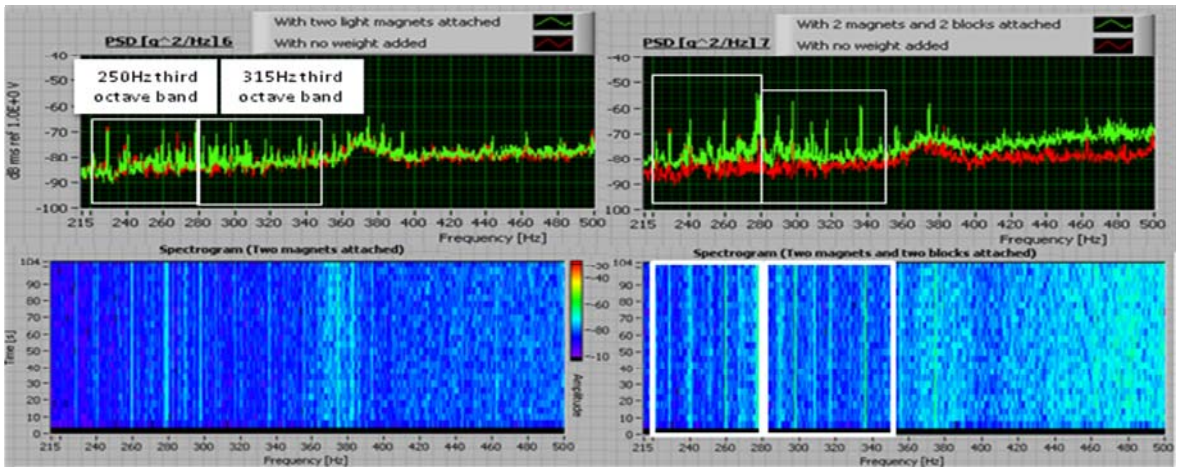

Figure 12. Power spectral density and the spectrogram in the frequency range 215-500 Hz, with two magnets attached to the shaft (left) and two magnets and two blocks (right).

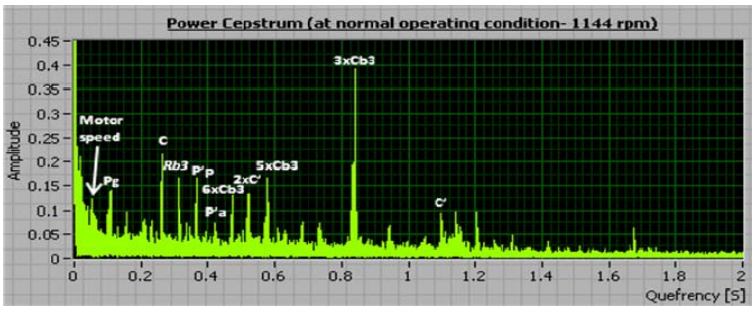

Figure 13. Forcing frequencies identification on the Cepstrum plot.

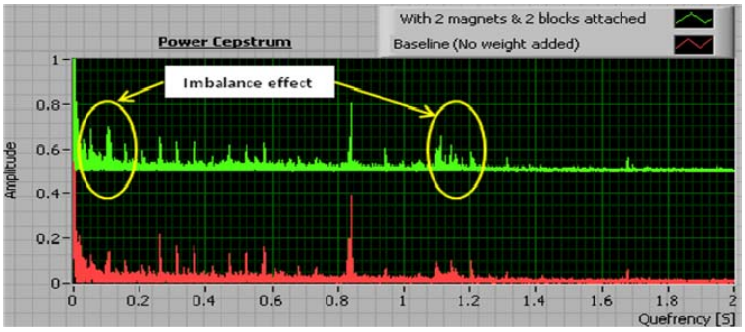

Figure 14. Cepstrum averaged over 25 samples (motor running at 1,144 RPM)-baseline (blue) shifted up by 0.5 compared to extreme imbalance case (green)

Cepstrum analysis was evaluated for early detection or fault diagnosis. In Figures 13 and 14, the increased imbalance of the shaft caused by the weight resulted in amplitude increases of the harmonically related frequencies. These changes are difficult to assess because the imbalance changes the dynamics of the system; e.g., the stress localized on a tooth due to the imbalance of the shaft produces modulation of the tooth-meshing frequencies with the shaft speed. Also, a large number of sidebands around the tooth-meshing frequency and its harmonics in the spectrum are generated, which are spaced by the rotation frequency of the shaft. As discussed earlier, the use of the Hilbert transform based techniques allows for easier interpretations to the monitoring of the envelope at specific frequencies, such as bearing or gear related frequencies. The easier interpretation increases the probability of early detection.

5. TRANSIENT ANALYSIS

A transient analysis utilizing kurtosis and STFT was performed using a calibrated hammer. The hammer hit the structure every second with increasing intensity over 96 seconds; a significant increase in the kurtosis and spikes on the spectrograms were observed. Figure 15 shows the time waveforms (green curve in normal operating condition and yellow curve with hammer tests) and the hammer forces (red curve) recorded during 96 seconds, the kurtosis and the short time Fourier transforms for several different conditions. Spectrograms on the top of the figure show the STFT resulting from normal operating condition; the kurtosis was 3.32 for each stage. Spectrograms on the bottom show the STFT for the extra light hammer hits (4 to 36 s), for light hammer hits (36 to 68 s) and strong hammer test (68 to 100 s), respectively. The time step and frequency resolution of the STFT were set to 0.125 s and 8 Hz, respectively.

The hammer hits experiment was performed on the coupled dynamometer (Figure 2). As the vibration level increases with the RPM, the hammer hits should be larger in high speed than in lower speed (to avoid being masked by the vibration level). The speed of the drive motor was selected to be 300 RPM (low speed) to avoid damage to the gearbox. Table 5 shows the amplitude change relative to the baseline (no hammer hits) of the kurtosis in the case of extra light, light and strong hammer hits.

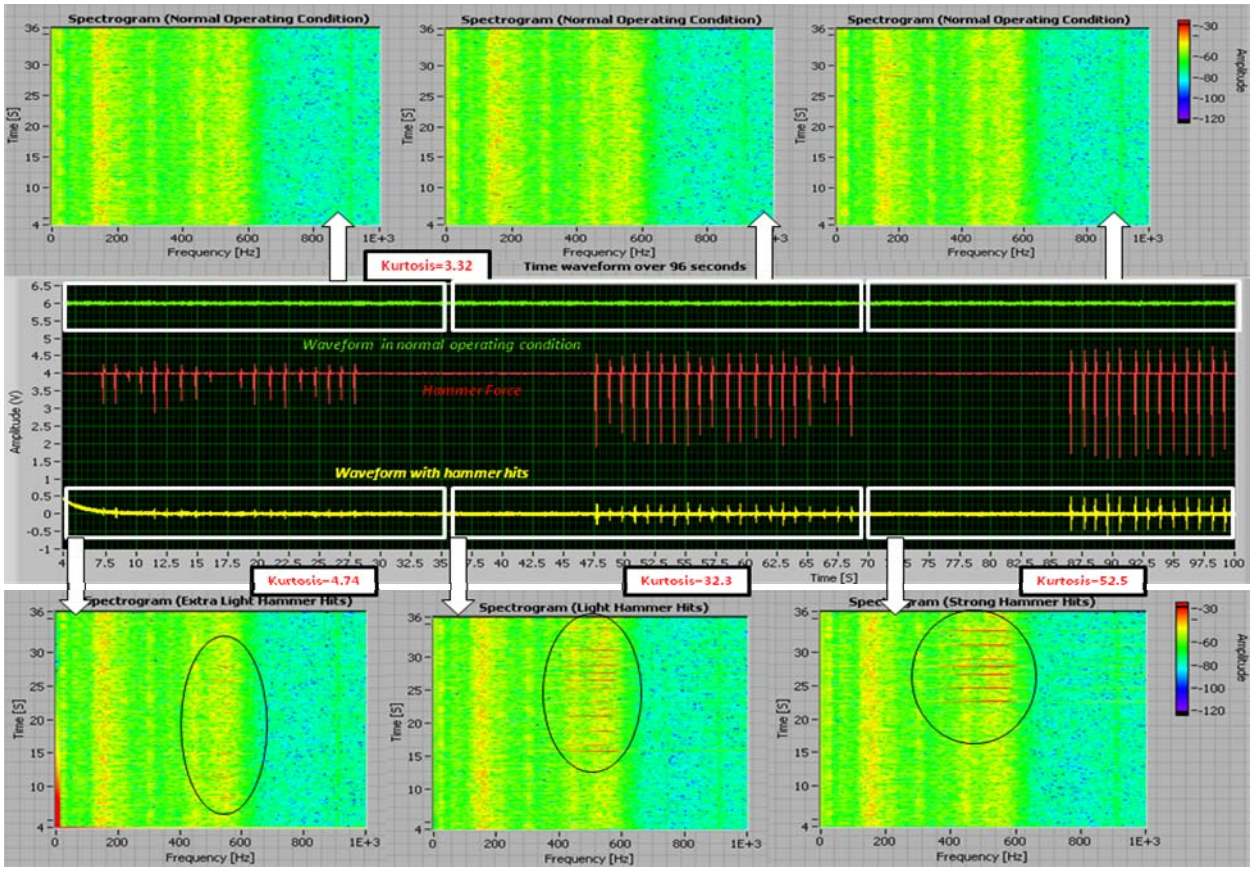

Figure 15. Spectrogram and kurtosis of the time waveform, for extra light (4-32 s), light (36-68 s) and strong hammer hit (68-100 s) at 300 RPM. Curve in red represents the hammer force. Yellow and green curves are the time waveform, with hammer test and in normal operating condition respectively.

	Relative Kurtosis
Extra light hammer hits	1.42
Light hammer hits	28.98
Strong hammer hits	49.18

Table 5. Relative kurtosis to the baseline for increasingly stronger hammer hits.

6. CONCLUSION

During the process of data acquisition and processing, several findings were made that are believed noteworthy:

(1) Augmenting the imbalance caused the planet gear meshing frequency to be modulated by the output shaft speed of the second stage reduction gearbox (0.88 Hz for 1,144 RPM and 1.25Hz for 1595). The modulation level increased with increased imbalance.

(2) The PSD was a better indicator of level change than the cepstrum, although the cepstrum is a better tool to identify harmonic relationships.

(3) Envelope analysis using Hilbert transform techniques is a better indicator of modulation content than the PSD and the cepstrum; this is consistent with reference (Fernandez et al., 2005). It may outperform the kurtosis analysis in the presence of transients.

(4) The kurtosis seems to be a good indicator for transient effects; the kurtosis had similar values with and without imbalance. However, had the imbalance been introduced while the shaft was rotating (transient), the value of the kurtosis would have changed significantly. Also, the kurtosis would have been increased if the imbalance had caused gear or bearing damages.

(5) The envelop analysis was performed on the planet gear meshing frequency. The results were similar to those found in (Fernandez et al., 2005; Yong-Han Kim et al., 2006) using bearing frequencies.

(6) The data comparisons indicate that the use of more than one technique for fault detection and identification increases the reliability of the conclusions. This might decrease the false alarms rate and the use of lower alarms levels, allowing for earlier fault detection.

In the light of these findings, the use of envelop and kurtosis analyses for detection of bearing and gear related

faults should be considered in addition to PSD levels. This allows for more reliable of fault identification and for evaluation of the severity of the problem.

REFERENCES

Beaujean, P.-P. J., Khoshgoftaar, T. M., Sloan, J. C. Xiros, N. & Vendittis, D. (2009). Monitoring Ocean Turbines: a Reliability Assessment. In *Proceedings of the 15th ISSAT International Conference on Reliability and Quality in Design*.

Driscoll, F. R., Skemp, S. H., Alsenas, G. M., Coley, C. J. & Leland A. (2008). Florida Center for Ocean Energy Technology. In *Proceedings of the MTS/IEEE Oceans'2008.*

Fernandez, A., Bilbao J., Bediaga I., Gaston, A. & Hernandez, J., (2005). *Feasibility study on diagnostic methods for detection of bearing faults at an early stage*. In *Proceedings of the WSEAS Int. Conf. on dynamical systems and control*.

Fan, X. & Zuo, M.J. (2006). *Gearbox fault detection using Hilbert and wavelet packet transform*. Mechanical Systems and Signal Processing, 20, 966–982.

Singleton, K. (2006). *Case Study, Two Stages Planetary Gearbox*. www.vibration.org.

Kim, Y.-H., Tan, A. C. C., Mathew, J. & Yang, B.-S. (2006). *Condition monitoring of low speed bearings: a comparative study of the ultrasound technique versus vibration measurements*. In *Proceedings of the World Congress on Engineering Asset Management*.

Mjit, M. (2009). *Methodology for fault detection and diagnostics in an ocean turbine using vibration analysis and modeling*. Master's thesis. Florida Atlantic University.

Mjit, M., Beaujean, P.-P.J. & Vendittis, D. J. (2010). *Fault Detection and Diagnostics in an Ocean Turbine using Vibration Analysis*. In *Proceedings of ASME IMECE10*.

Reimche, W., Südmersen, U., Pietsch, O., Scheer, C., Bach, F.-W. (2003). *Basics of Vibration Monitoring For Fault Detection and Process Control*. In *Proceedings of the 111 Pan-American Conference for Non-Destructive* Testing.

Sloan, J. C., Khoshgoftaar, T. M., Beaujean, P.-P. J. & Driscoll, F. (2009). Ocean Turbines – a Reliability Assessment. *International Journal of Reliability, Quality and Safety Engineering*, 16(5), 1-21.

Tyagi, S. (2003). *Wavelet Analysis And Envelope Detection For Rolling Element Bearing Fault Diagnosis, A Comparative Study.* In *Proceedings of the 11th National Conference on Machines and Mechanisms.*

Wald, R., Khoshgoftaar, T. M., Beaujean, P.-P. J., & Sloan. J. C. (2010). Combining wavelet and Fourier transforms in reliability analysis of ocean systems. In *Proceedings of the 16th ISSAT International Reliability and Quality in Design Conference*.

Mustapha Mjit is an engineer in structural vibrations for the Southeast National Marine Renewable Energy Center at Florida Atlantic University. He earned his M.S. degree in Ocean Engineering at Florida Atlantic University (2009) and his Master's in Mechanical Engineering at the Université de Technologie de Compiegne, France (2006). In 2010, he received a fellowship award from Siemens Energy under the Gas Turbine Industrial fellowship Program. His professional experience includes vibration and health monitoring of rotating machines. Mustapha Mjit is a member of SNAME (2009), Tau Beta Pi Engineering Honor Society (2010) and Ordre des Ingénieurs du Québec (2010).

Dr. Pierre-Philippe J. Beaujean is an associate professor at Florida Atlantic University in the Department of Ocean and Mechanical Engineering. He received his Ph.D. in Ocean Engineering at Florida Atlantic University in 2001. He specializes in the field of underwater acoustics, signal processing, sonar design, data analysis, machine-health-monitoring and vibrations control. Dr. Beaujean is an active IEEE, ASA and MTS member.

Dr. David J. Vendittis [Ph.D. (Physics) - American University, 1973] is a Research Professor (part time) at the Center for Ocean Energy and Technology, Florida Atlantic University. Additionally, he is the Technical Advisory Group (ASA/S2) chairman for an International Standards Organization subcommittee, ISO/TC108/SC5 - Machinery Monitoring for Diagnostics. This committee writes international standards that support Machinery Condition Monitoring for Diagnostics. He was appointed to this position by the Acoustical Society of America.